ARTICLE

Electrical Properties of Outer Membrane Extensions from Shewanella Oneidensis MR-1

Received 00th January 20xx,
Accepted 00th January 20xx

DOI: 10.1039/x0xx00000x

Helena Lozano[a], Ruben Millan-Solsona[a,b], Nuria Blanco-Cabra[c], Rene Fabregas[d], Eduard Torrents[c,e], Gabriel Gomila[*,a,b]

Shewanella oneidensis MR-1 are metal-reducing bacterial cells able to exchange electrons with solid-phase minerals outside the cell. These bacterial cells can produce outer membrane extensions (OMEs) that are tens of nanometer wide and several microns long. The capability of these OMEs to transport electrons is currently under investigation. Chemically fixed OMEs from *S. oneidensis* have shown good dc conducting properties when measured in air environment. However, no direct demonstration on the conductivity of intact (non-chemically fixed) OMEs has been provided, yet, due to the inherent difficulties in measuring it. In the present work, we measured the electrical properties of intact OMEs in dry air environment by using Scanning Dielectric Microscopy (SDM) in force detection mode. We found that at the frequency of the measurements (~2 kHz), OMEs show an insulating behavior, with an equivalent homogeneous dielectric constant ε_{OME} = 3.7 ± 0.7 and no dephasing between the applied ac voltage and the measured ac electric force. The dielectric constant measured for the OMEs is comparable to that obtained for insulating supramolecular protein structures ($\varepsilon_{protein}$ = 3-4), pointing towards a rich protein composition of the OMEs, probably coming from the periplasm. Based on the detection sensitivity of the measuring instrument, the upper limit for the ac conductivity of intact OMEs in dry air environment has been set to $\sigma_{OME,ac}<10^{-6}$ S/m, a value several orders of magnitude smaller than the dc conductivity measured in air environment in chemically fixed OMEs. The lack of conductivity of OMEs can be attributed to the relatively large separation between cytochromes in non-chemically fixed OMEs and to a suppression of the cytochromes' mobility due to the dry environmental conditions.

A Introduction

Some bacterial species such as *Geobacter sulfurreducens*, *Shewanella oneidensis* and several others can exchange electrons extracellularly with solid electrodes or minerals (*1*), (*2*), (*3*). Electrons are exchanged by direct contact with the substrate, through molecular shuttles, like flavins, or through cell appendages, such as pili, outer membrane extensions or protein fibers (*3*), (*4*). The bacterial cell appendages act as conduits of electrons between the cell and distant substrates and for this reason they are referred to as bacterial nanowires (*5*), (*6*), (*7*), (*8*), (*9*), (*10*), (*11*), (*12*). Bacterial nanowires enable the exchange of electrons with substrates located microns far from the cell body. Their existence has attracted a lot of attention in the field of bioelectronics due to their unique and fascinating potential applications (*13*), (*14*), (*15*).

Outer Membrane Extensions (OMEs) from *Shewanella oneidensis MR-1* have been suggested to be bacterial nanowires (*16*). OMEs are produced from the controlled blebbing of the outer membrane of the bacterial cell under oxygen limitation growth conditions (*16*), (*17*). They are composed of proteins and lipids, with no presence of RNA or chromosomal DNA (*18*). They are microns long and their diameter ranges from ~40 nm to ~250 nm (*17*). Different studies have demonstrated that chemically fixed *S. oneidensis* OMEs conduct electricity in an air environment. Conductivities of up to ~1 S/cm have been reported (*7*). The charge transport mechanism is believed to be multistep electron hopping between cytochromes (*19*). The hopping conduction is made possible because cytochromes are closely packed in these systems, since the growth under oxygen limitation condition increases the density of cytochromes and the chemical fixation reduces the diameter of the OMEs down to only ~10 nm (*6*), (*20*). The charge transport presents a p-type tunable electronic behavior (*10*). For non-chemically fixed OMEs no direct evidence of their conductive properties has been provided, yet. Measuring the conductivity of intact (non-chemically fixed) OMEs is very challenging, since two-electrode

[a] *Nanoscale bioelectric characterization, Institut de Bioenginyeria de Catalunya (IBEC), The Barcelona Institute of Science and Technology (BIST), c/ Baldiri i Reixac 11-15, 08028, Barcelona, Spain.*
[b] *Departament d'Enginyeria Electrònica i Biomèdica, Universitat de Barcelona, c/ Martí i Franqués 1, 08028, Barcelona, Spain.*
[c] *Bacterial infections and antimicrobial therapies, Institut de Bioenginyeria de Catalunya (IBEC), The Barcelona Institute of Science and Technology (BIST), c/ Baldiri i Reixac 11-15, 08028, Barcelona, Spain.*
[d] *Department of Physics and Astronomy, University of Manchester, Manchester M13 9PL, UK.*
[e] *Departament de Genètica, Microbiologia i Estadística, Universitat de Barcelona, Av. Diagonal 643, 08028, Barcelona, Spain*

Electronic Supplementary Information (ESI) available: Additional data to Figure 1a. Effect of hydration on the OMEs physical dimensions. Additional data to Figure 2c. Additional data to Figure 3. Effect of the shell conductivity on the dC/dz values for a core-shell model of the OMEs. OMEs growth reactor. See DOI: 10.1039/x0xx00000x

or Conductive Atomic Force Microscopy (C-AFM) measurements are difficult to be performed in such fragile nanostructures. Indirect evidence on their possible conductive nature has been provided using ultrastructural cryo-Transmission Electron Microscopy (cryo-TEM) and Fluorescence Microscopy studies, which demonstrate that the density and mobility of cytochromes in the OMEs could enable electronic hopping conduction assisted by the diffusion of the cytochromes in the OMEs (*17*).

In order to shed more light on this open problem, here, we measured the ac electric properties of intact, non-chemically fixed, *Shewanella oneidensis* OMEs in dry air environment using Scanning Dielectric Microscopy (SDM) in force detection mode (*21*). SDM measures the ac electric force acting on the conductive probe of an Atomic Force Microscope (AFM) in response to an ac voltage applied between the probe and the sample's substrate. The measured electric force senses the ac polarization properties of the nanoscale object, which depends on its ac conductivity and dielectric constant, whose values can be obtained following a stablished procedure. SDM, being a non-contact nanoscale electrical technique, is especially well suited to determine the electrical properties of fragile nanoscale objects like non-chemically fixed OMEs. Studies on the conductive and dielectric properties of nanoscale objects by means of SDM have been carried in the past on carbon nanotubes (*22*), (*23*), (*24*), inorganic semiconducting (*25*) and metallic (*26*) nanowires, single metallic (*27*) and dielectric (*21*) nanoparticles, single virus particles (*21*) and macromolecular protein structures such as virus capsids and tails (*28*), and bacterial flagella (*29*). Recently, SDM has also been applied to support the electrical conduction properties of protein fibers in filamentous cable bacteria (*30*).

B Results

OMEs from *S. oneidensis* MR-1 bacterial cells were produced as previously described in Ref. (*16*) (see Materials and Methods). Figure 1a shows a fluorescence optical microscopy image of the bacterial cells adsorbed on a glass coverslip labelled with the membrane FM™ 4-64FX dye. OMEs (some of which are highlighted with white arrows) can be clearly identified in several bacterial cells (additional images are provided in the Supporting Information S1). Figure 1b shows a topographic AFM image of a sample prepared on a gold-coated glass coverslip and imaged in a dry air environment in intermittent contact mode. Again, OMEs can be identified in several of the bacterial cells (some of which are highlighted by white arrows). Figure 1c shows a zoom-in AFM image around one of the OMEs. The OME shows the characteristic bubbling structure formed by a chain of small vesicles ~ 40 – 80 nm in diameter (see cross-section topographic profile in the inset of Fig. 1c), in agreement with results reported earlier from cryo-TEM imaging (*16*). We note that the drying process does not seem to affect significantly the size of the OMEs. To show it we have acquired AFM images of dry and re-hydrated OMEs and observed that their size remains not much affected, while for instance, that of the bacterial cell nearly doubles (see Supporting Information S2). This result suggests that the distribution of cytochromes in non-chemically fixed dry OMEs could be like the one found in hydrated or flash-frozen samples, although a more direct demonstration would be required to confirm it.

To measure the electric polarization properties of the OMEs by means of SDM (*21*) we have applied an ac voltage of frequency f_{el}~ 2 kHz and amplitude v_{ac} = 5 V between the conductive AFM probe and the conducting substrate in dry air environmental conditions. The applied electric potential induces the oscillation of the cantilever. The amplitude and dephasing of the $2f_{el}$ harmonic is measured as a function of distance on selected positions of the sample. From the oscillation amplitude we derive the values of the capacitance gradient value, dC/dz, which contain the information on the electric polarization properties of the OMEs (*21*) (see also Materials and Methods).

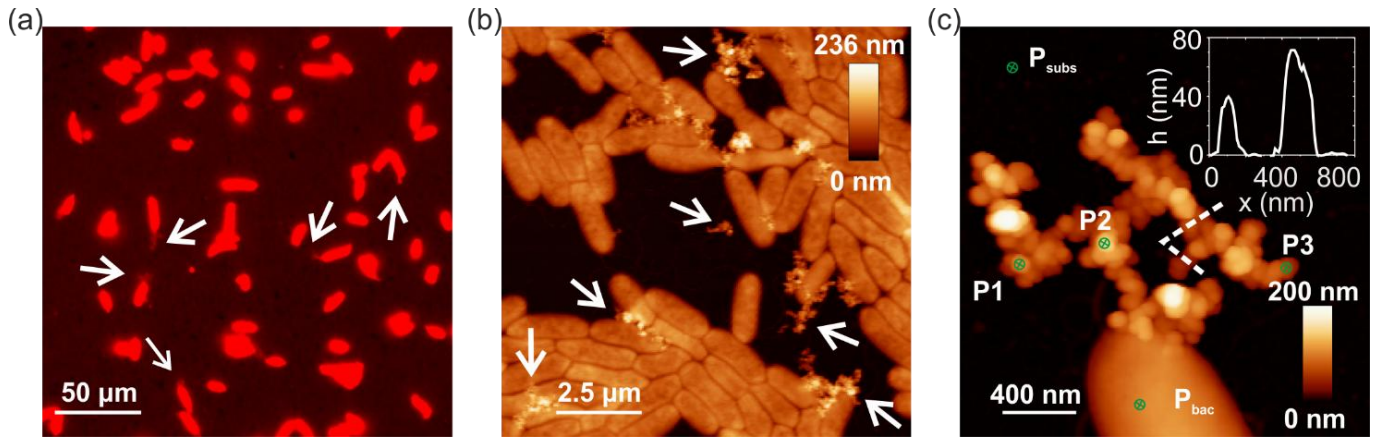

Figure 1. (a) Fluorescence light microscope image of S. oneidensis bacterial cells labelled with the membrane dye FMTM 4-64FX dye. White arrows point towards some of the OMEs. (b) AFM topographic image of S. oneidensis bacterial cells in an air environment. OMEs are marked with white arrows. (c) Zoom in AFM image of one of the OMEs showing its characteristic bubbling structure. Inset: Topographic cross-section profile of the OME along the white dashed line in (c).

ARTICLE

Figure 2a shows capacitance gradient *dC/dz* versus tip substrate distance, *z*, curves acquired at the five positions marked in Fig. 1c, namely, P_{subs} (substrate), P1-P3 (OME) and P_{bac} (bacterial cell body). At a given tip-substrate distance, z, the *dC/dz* values measured on the OME (and on the bacterial cell) are higher than those measured on the bare metallic substrate (black line). This fact just reflects that the polarization of the OMEs (and of the bacterial cell) is detected and that it is higher than that of the air environment (as should be). We also note that for large tip-substrate distances, z > 300 nm, all the *dC/dz* curves merge with that of the substrate. This fact is an indication that the electric measurements are local for z < 300 nm. The inset of Fig. 2a shows the dephasing measured between the cantilever oscillation 2ω-harmonic and the ac applied voltage as a function of the tip substrate distance (see Materials and Methods for details). No dephasing is observed in none of the locations where measurements have been performed and for none of the tip-substrate distances considered. From the results reported in Fig. 2a, some conclusions can be drawn. First, the lack of dephasing between the cantilever oscillation 2ω-harmonic and the ac applied voltage is a signature of either an insulating or a highly conductive behavior (*30*). This fact discards a poor conductor or a lossy dielectric behavior, since in those cases some dephasing should be observed (see discussion section). Furthermore, we note that the *dC/dz* versus distance curve measured on the OME at point P3 is almost identical to that measured on the bacterial cell body at point P_{bac} (orange and green continuous lines in Fig. 2a). Since the heights of them are almost the same, these results indicate that the OME polarization response is like that of a bacterial cell in a dry air environment. In Ref. (*31*) we showed that under this condition bacterial cells show an insulating behavior at the frequency of the measurements with an equivalent homogeneous dielectric constant $\varepsilon_{bac} \sim 3 - 4$. One, therefore, would expect a similar behavior for the OMEs.

We have quantified the *dC/dz* versus tip-substrate distance curves in Fig. 2a to extract the equivalent homogeneous dielectric constant of the OMEs (and of the bacterial cell), ε_{eq}, following the standard quantitative procedures of SDM (*21*), (*32*), (*33*). In a nutshell, theoretical *dC/dz* vs distance curves have been calculated for a tip-OME homogeneous dielectric model and fitted to the experimental *dC/dz* curves, with the equivalent homogeneous dielectric constant, ε_{eq}, as single fitting parameter. The geometrical model of the OMEs has been extracted directly from the measured sample topography, as described elsewhere (*34*). Figure 2b shows an example of one of the tip-sample geometries modelled to quantitatively analyze the *dC/dz* curves, corresponding to position P2 in Fig. 1c. The tip is assumed to be a cone with a tangent sphere apex, with their dimensions being obtained from the *dC/dz* vs distance curves measured on the bare metallic substrate, as described elsewhere (*21*), (*32*), (*33*), (*35*). In Fig. 2b, we show an example of a calculated electric potential distribution displayed on the surface of the OME, which highlights the locality of the SDM measurements.

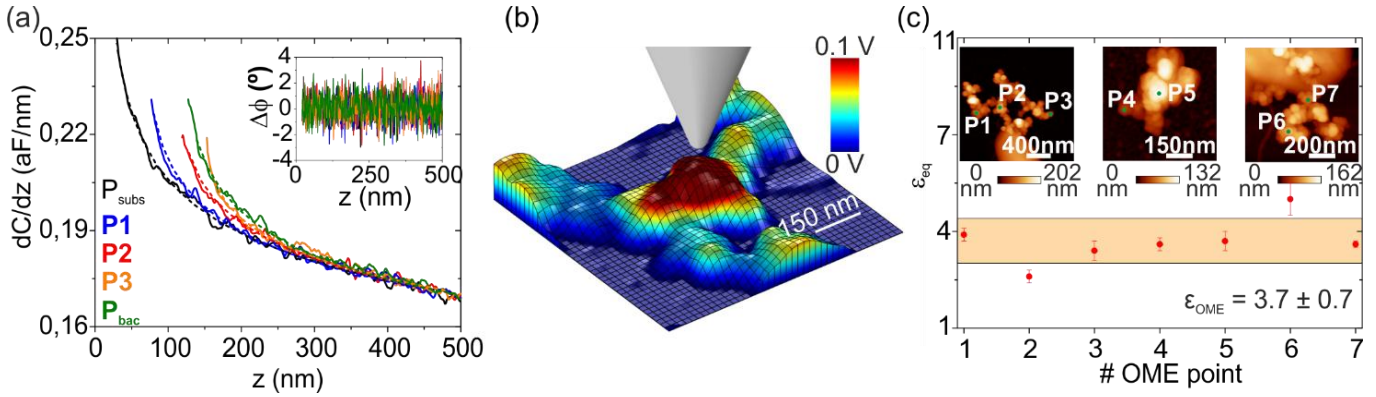

Figure 2. (a) Capacitance gradient (from the 2ω-electric force harmonic) versus tip-substrate distance curves measured on the selected positions of the sample in Fig. 1c (Psubs substrate, P1-P3 OME, and Pbac bacteria cell body). All curves are plotted as a function of the tip-substrate distance. The dashed lines represent the fitted numerically calculated curves. Inset: Dephasing between the 2ω-electrical force harmonic and the ac applied voltage as a function of the tip-substrate distance. Experimental parameters: $v_{ac} = 5$ V, $f_{el} = 2$ kHz, Gain = 1, tip = PtSi-CONT and k = 0.3 N/m. (b) Example of a tip-OME geometrical model (corresponding to P3) used to compute the theoretical dC/dz approach curves. One of the calculated electric potential distributions is plotted on its surface. Tip parameters used in the calculations (obtained from the dC/dz curve measured at Psubs): tip radius R = 23 nm, half cone angle θ = 20°, capacitance gradient offset $C'_{offset} = 97$ zF/nm. The remaining parameters of the tip were set to their nominal values: cone height H = 12.5 μm, local cantilever length $L_c = 3$ μm and cantilever thickness $W_c = 3$ μm. (c) Summary of the equivalent homogeneous dielectric constants, ε_{eq}, extracted on three different OMEs. The insets show the topographic AFM images of the OMEs with the location of the points at which the electrical measurements have been performed. The first inset AFM image is the same as that of Fig. 1c, reproduced here for an easier reference.

The dashed lines in Fig. 2a correspond to the fitted theoretical curves obtained following this procedure (note that for each point P1-P3 the corresponding local sample topography has been used in the modelling). The equivalent homogeneous dielectric constant values obtained are: $\varepsilon_{P1} = 3.9 \pm 0.2$, $\varepsilon_{P2} = 3.4 \pm 0.3$, and $\varepsilon_{P3} = 2.6 \pm 0.2$. The errors have been estimated from the sensitivity of the *dC/dz* values to the dielectric constant for an instrumental noise of 1 zF/nm. The averaged equivalent homogeneous dielectric constant for this OME is $\varepsilon_{OME} = 3.5 \pm 0.8$. This value is like the one obtained for the bacterial cell at position P_{bac} (by using a bacterial model) $\varepsilon_{bac} = 3.9 \pm 0.1$, thus confirming the veracity of the qualitative argument made above. The dielectric nature of the model considered in this quantitative analysis also predicts the lack of dephasing between the 2ω-harmonic oscillation and the applied ac voltage, in agreement with the lack of dephasing found in the experiments. The same analysis has been repeated for two additional OMEs corresponding to different bacterial cells (see Supporting Information S3). A summary of the equivalent homogeneous dielectric constants extracted is shown in Fig. 2c. The topographic images corresponding to each OME, and the locations where the electrical measurements have been performed, are shown as insets. For the three OMEs analyzed, similar values for the dielectric constant, ε_{eq}, have been obtained. The overall averaged dielectric constant value obtained is $\varepsilon_{OME} = 3.7 \pm 0.7$, where the error is the standard deviation over the N = 7 measurements corresponding to seven different locations on the three different OMEs.

To assess the uniformity of the dielectric properties of the OMEs we have acquired lift-mode SDM images and analyzed them quantitatively. Figure 3a shows the AFM topographic image of one of the regions analyzed (located around point P2 in Fig. 1c). Figures 3b and 3c show, respectively, the corresponding lift-mode *dC/dz* and phase SDM images acquired at a lift distance z = 55 ± 2 nm with respect to the sample surface.

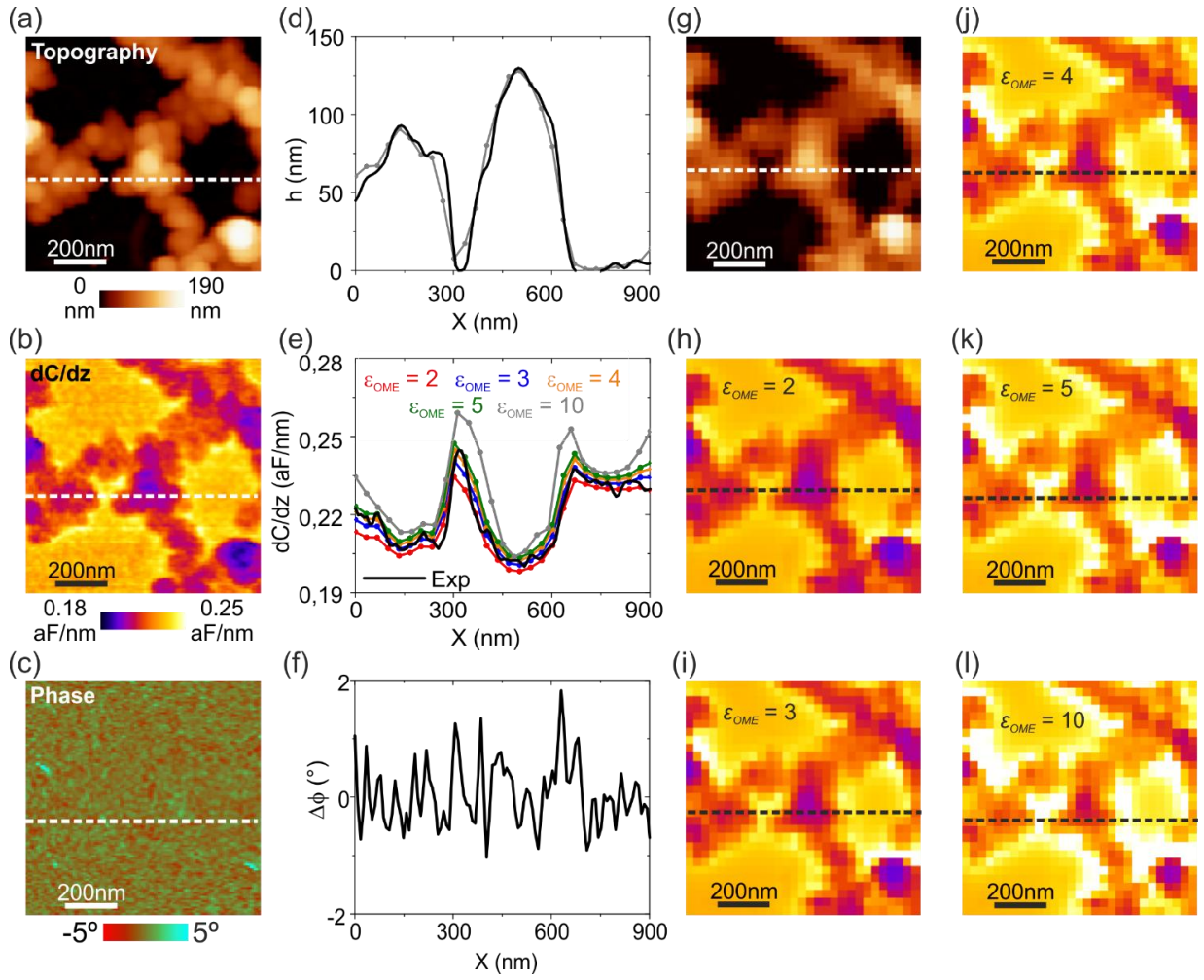

Figure 3. (a) Topographic AFM image of the OME located around point P2 in Fig. 1c. (b) Corresponding lift-mode dC/dz and (c) phase SDM images at a distance z = 55 nm from the sample surface, respectively. Experimental parameters: $v_{ac} = 5$ V, $f_{el} = 2$ kHz, Gain = 1, tip = PtSi-CONT and k = 0.3 N/m. Cross-section profiles of the (d) topography, (e) dC/dz and (f)

phase along the dashed lines in (a)-(c), respectively (solid black lines). The grey line with symbols in (d) corresponds to the topographic profile along the dashed line in the reduced topographic model in (g). The solid lines with symbols in (e) correspond to calculated theoretical dC/dz cross-section profiles along the dashed lines in (h)-(l). (g) Reduced 29x29 pixel topographic model used for the numerical calculations. (h)-(l) Lift-mode dC/dz images calculated with the reduced geometrical model in (g) for different values of the equivalent homogeneous dielectric constant of the OME, ε_{OME} = 2, 3, 4, 5 and 10, respectively. In all calculated cases, the dephasing is null (not shown). Tip parameters: same as in Fig. 2.

The lift-mode *dC/dz* image (Fig. 3b) shows an excellent contrast, although a substantial part of it comes from topographic crosstalk effects, as discussed elsewhere (*36*). The phase image shows no contrast at all, confirming the lack of dephasing induced by the OMEs between the ac electric force and the ac applied voltage. Figures 3d-3f (black lines) show cross-section topographic, capacitance gradient, *dC/dz*, and dephasing profiles taken along the dashed lines in Figs. 3a-3c. To quantitatively analyze the lift-mode electric image, we have built a geometric model for the OME extracted from the topographic image in Fig. 3a and moved the tip along it at a constant tip-sample distance to form the corresponding *dC/dz* lift-mode images. For computational efficiency, a reduced number of pixels (29x29) have been included in the geometric model, see Fig. 3g. Despite the reduction in the number of pixes, the geometric model still describes the topography of the OMEs faithfully (see Fig. 3d for a comparison of the topographic cross-section profiles obtained from the experimental and simulated reduced topographic images). Figures 3h-3l show calculated lift-mode *dC/dz* images for five values of the homogeneous equivalent dielectric constant of the OME, ε_{OME} = 2, 3, 4, 5, 10. By comparing the calculated images (Figs. 3h-3l) with the experimental one (Fig. 3b), we observe that the best matching is obtained for ε_{OME} = 3 – 4 (see also the comparison of the calculated and experimental *dC/dz* cross-section profiles in Fig. 3e and the histogram analysis in the Supporting Information S4). This result agrees with what obtained from the electrical measurements on selected locations (see Fig. 2c) and that gave ε_{OME} = 3.7 ± 0.7. This result confirms that the dielectric response of the OMEs is rather uniform and discards the presence of spots or regions with different dielectric behavior. Since the model is purely dielectric, it predicts no dephasing, in agreement with the experimental measurements.

C Discussion

We have measured the ac electrical properties of intact, non-chemically fixed, Outer Membrane Extensions (OMEs) from *S. oneidensis* MR-1 bacterial cells by means of Scanning Dielectric Microscopy (SDM) in dry air environment. We have found that at the frequency of the measurements (~2 kHz) the homogeneous equivalent dielectric constant of the OMEs is ε_{OME} = 3.7 ± 0.7. Furthermore, no dephasing between the measured ac electric force and the applied ac voltage has been observed. These results indicate that intact OMEs in a dry air environment, and at the measuring frequency of ~2 kHz, show an insulating behavior. The measured equivalent homogeneous dielectric constant reflects, then, the composition of the OMEs (*21*). OMEs have a bubbled core-shell structure, with a membrane composed mainly by lipids and polysaccharides (like the outer cell membrane) and a core filled with periplasm content consisting of a gel of densely packed proteins (*16*) , (*17*). The thickness of the membrane is only ~5 nm, much smaller than the actual size of the OMEs (~40-80 nm). Moreover, the polarizability of the membrane components is lower to that of proteins (lipids and lipopolysaccharides have dielectric constants in the range ε_r ~ 2 – 3, while proteins have $\varepsilon_{proteins}$ ~ 3 – 4 (*28*), (*37*), (*29*)). These facts imply that the equivalent homogeneous dielectric constant of the OMEs is basically determined by the dielectric constant of the proteins in the core. This result explains, then, why the measured dielectric constant of the OMEs (ε_{OME} = 3.7 ± 0.7) is similar to that measured on other supramolecular insulating protein structures ($\varepsilon_{proteins}$ ~ 3 – 4). On the other side, for the case of conductive protein fibers, as those present in filamentous cable bacteria, it has been shown that the equivalent homogeneous dielectric constant is much higher (ε_{cable} = 11 ± 3), what is compatible with a conductive core-insulating shell model (*30*).

We have analyzed whether the measured electrical forces for the OMEs are compatible with the presence of some relevant conductivity in the OMEs. To this end we followed a similar procedure to the one described in Ref. (*30*). We have considered a dielectric homogeneous model like the one in Fig. 2b, and added to it an equivalent homogeneous conductivity, σ_{OME}. Figures 4a-4c (res. Figs. 4d-4f) show surface (res. cross-section) electric potential distributions calculated for this model for three characteristic conductivities $\sigma_{OME} = 10^{-8}$ S/m, $\sigma_{OME} = 10^{-6}$ S/m and $\sigma_{OME} = 10^{-5}$ S/m, corresponding, respectively, to insulator, lossy insulator and conductor behaviors (see below). It is observed that the presence of just minute conductivities would largely alter the electric forces measured by the tip. Figures 4g and 4h show the values of the *dC/dz* contrast and dephasing, respectively, as a function of the conductivity of the OME for a frequency of 2 kHz and for a tip-substrate distance z = 196 nm. The results show that for conductivities $\sigma_{OME} < 10^{-7}$S/m the OME shows an insulating behavior with *dC/dz* being independent of the conductivity, σ_{OME}, and strongly dependent on the dielectric constant, ε_{OME}. No dephasing is obtained in this conductivity range. For conductivities $\sigma_{OME} > 10^{-5}$ S/m, the OME shows already a "full" conductive behavior, with *dC/dz* being independent from both the conductivity and the dielectric constant. No dephasing is predicted for this range of conductivities neither. Finally, in the intermediate range of conductivities 10^{-7} S/m< $\sigma_{OME} < 10^{-5}$ S/m the OME behaves like an insulator with loses, with *dC/dz* being dependent on both the dielectric constant and the conductivity. A non-null dephasing of a few degrees is obtained in this case.

ARTICLE

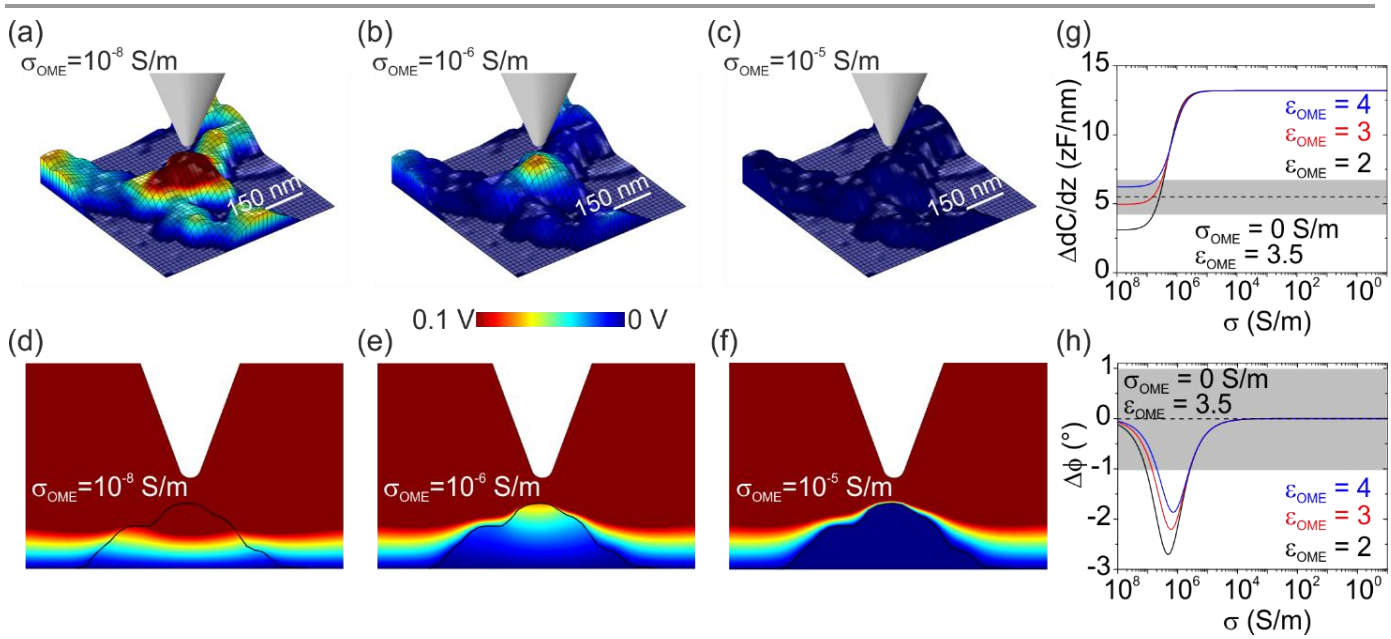

Figure 4. (a)-(c) Calculated electrical potential distribution overlaid on the surface of a conductive homogeneous OME model around point P2 from Fig. 1c, for three characteristic conductivities $\sigma_{OME} = 10^{-8}$ S/m (insulator), $\sigma_{OME} = 10^{-6}$ S/m (insulator with losses) and $\sigma_{OME} = 10^{-5}$ S/m (conductor). (d)-(f) Corresponding cross-section electric potential distributions. (g) Capacitance gradient and (h) dephasing as a function of the conductivity of the OME for three different values of the dielectric constant of the OME. The dashed line corresponds to the value of a pure dielectric model with a dielectric constant equal to the experimentally determined value. The grey area represents the noise of the measuring instrument. Parameters: R=23 nm, θ=20º, H=12.5 μm, L_c=W_c=3 μm, z=196 nm, 41 x 41 pixel.

The grey band in Fig. 4g and 4h represent the experimental values for the *dC/dz* contrast and the dephasing under uncertainty corresponding to the experimental values ($\varepsilon_{OME} \sim 3.5$ and $\sigma_{OME} \sim 0$ S/m, dashed lines in Figs. 4g and 4h, and $dC/dz_{noise} \sim 1$ zF/nm and $phase_{noise} \sim 1°$). By analyzing the graphs, one can set that the upper conductivity limit compatible with the experiments for the OMEs is $\sigma_{OME} < 3 \times 10^{-7}$ S/m, a value very far from that reported in chemically fixed OMEs ($\sigma_{OME,fixed} \sim 1$ S/m) (*7*). We have performed a similar analysis for the case of considering a core-shell conductive model for the OMEs, which, in principle, should better reflect their actual structure (see Supporting Information S5). The core has been assumed to be insulating ($\sigma_{core} = 0$ S/m) with a dielectric constant $\varepsilon_{core} = 3$ (corresponding to proteins). The shell, instead, has been assumed to be conductive (e.g. due to the cytochrome hopping conduction) with conductivity σ_{shell}, and with a dielectric constant $\varepsilon_{shell} = 2$ (corresponding to lipids) and thickness, *d*. From the analysis performed, we obtained similar conclusions to the ones obtained with the homogeneous conductive model, namely, the maximum conductivity of the shell compatible with the experiments and the sensitivity of the measuring instruments is very low, in this case, $\sigma_{shell} < 10^{-6}$ S/m. From both the conductive homogeneous and core-shell models the upper limit of the conductivity for non-chemically fixed dry OMEs is orders of magnitude lower than the conductivity reported on chemically fixed dry OMEs ($\sigma_{OME,fixed} \sim 1$ S/m) (*7*). The absence of an ac conductivity in intact OMEs in dry air environment can be explained in terms of their structural and physical properties, which are different from those of dry and chemically fixed OMEs and from those of hydrated intact non-chemically fixed OMEs. Dry and chemically fixed OMEs show a strong reduction of its diameter during the sample preparation process passing from ~50 – 250 nm to just ~10 nm. The shrinking in size could drastically reduce the separation between cytochromes, which could eventually enable multistep hopping conduction, as discussed elsewhere (*19*), (*20*). Instead, in dry but non-fixed OMEs the diameter of the OMEs remains practically unmodified (see Supporting Information S2). As a result, the separation between the cytochromes is considerably larger than on fixed OMES, what would drastically reduce the hopping probability (which depends exponentially on the separation between hopping centers (*19*)). Furthermore, the diffusivity of the cytochromes in intact OMEs in dry air environment is also expected to be drastically reduced with respect to fully hydrated OMEs. This fact can prevent the occurrence of hopping conduction facilitated by the diffusivity of the hopping centers, which is the mechanism believed to take place in hydrated OMEs (*17*). The fact that the measurements

are performed in the kHz range can make the reduced diffusivity of the hopping centers even more very relevant. Altogether these facts can explain the lack of ac conductivity observed in the SDM measurements reported here. These results, however, do not imply that some conductivity cannot be observed on OMEs in hydrated natural conditions. As we mentioned above, in hydrated OMEs the cytochromes diffusivity is expected to be non suppressed, and hence could facilitate electron transport, at least at very low measuring frequencies, as it has been argued in Ref. (*17*). A direct demonstration of the conductive properties of intact OMEs in fully hydrated conditions is still challenging at present. A direct demonstration would require the realization of electric conductivity measurements in the liquid environment on intact OMEs. The possibility to operate SDM in the liquid environment has already been demonstrated (*38*), and applications on several fragile samples have been reported, like lipid bilayers (*39*), (*40*), self-assembled monolayers (*41*) or liposomes (*42*) and on electrolyte gated organic field-effect transistors (*43*). However, in-liquid SDM measurements need to be performed at frequencies in the MHz regime, which could make difficult the observation of diffusion assisted conductivity, which is expected to take place at lower frequencies. In addition, the preparation of intact OMEs in fully hydrated conditions for SDM measurements is challenging, due to the poor absorption of the OMEs on the conductive substrates required for SDM measurements. Further research is, then necessary, to overcome these issues.

D Experimental

Bacterial cell growth and preparation of OMEs samples. OMEs from *Shewanella oneidensis* MR-1 bacterial cells were produced as previously described in Ref. (*16*). *S. oneidensis* MR-1 (ATCC 700550) bacterial cells were grown overnight at 30°C in Luria-Bertani broth (LB) (Scharlab) in aerobic conditions. 5 ml of the overnight culture were centrifuged for 5 min at 4226 G, and the harvested bacteria were resuspended in the minimal defined medium (*16*) supplemented with 30 mM fumarate, and incubated anaerobically overnight at 30°C in Hungate tubes (purged with N_2). 50 ml of the anaerobic culture were again centrifuged for 5 min at 4226 G and resuspended in the minimal defined medium without fumarate. The resuspended bacterial cells were then placed in a reactor consisting of a glass cylinder pasted with silicone to a glass coverslip (or to a gold-coated glass coverslip) and let incubate for 3 – 4 hours at room temperature (see Supporting Information S6). The medium was then removed, and the sample was gently rinsed with miliQ water and left to dry at room temperature. Finally, the glass coverslip was removed from the reaction chamber. For fluorescence optical microscopy imaging, the glass coverslip was directly placed on the microscope. For SDM measurements, a gold-coated glass coverslip was used. In this case, after removing it from the reactor it was attached to a magnetic disk, which was connected on the one side to the gold surface, and on the other side to the ground of the AFM/SDM with a small wire by using silver paste.

Fluorescence images. Bacterial cells attached to the glass coverslip were stained with N-(3-triethylammoniumpropyl)-4-(6-(4-(diethylamino) phenyl) exatrienyl)pyridinium dibromide (FM™ 4-64FX, Thermo Fisher Scientific) at a concentration of 5 µg/ml, according to manufacturer instructions. Fluorescent images were acquired with a Nikon inverted fluorescent microscope ECLIPSE Ti-S/L100 (Nikon) equipped with a DS-Qi2 Nikon camera (Nikon).

Scanning Dielectric Microscopy. SDM measurements in force detection mode have been performed as described earlier (*21*). A Cypher S AFM system from Oxford Technologies (former Asylum Research) has been used with PtSi-CONT conductive probes (Nanosensors) with a typical spring constant $k \sim 0.2$ N/m, determined by the provider according to the probe dimensions, resonance frequency $f_r \sim 13$ kHz and nominal tip radius $R \sim 20$ nm. An ac voltage of amplitude $v_0 \sim 5$ *V* and frequency $f_{el} \sim 2$ kHz, much smaller than the resonance frequency of the cantilever, was applied between the probe and the conducting substrate. The amplitude, $A_{2\omega}$, and phase, $\phi_{2\omega}$, of the oscillation 2ω-harmonic was measured by using the system internal lock-ins (for further details see Ref. (*29*)). The overall conversion of raw $A_{2\omega}$ data to capacitance gradient values *dC/dz* values was done by using the relation (*21*)

$$\frac{dC}{dz} = \frac{4}{v_{ac}^2} k \frac{(A_{2\omega} - A_{2\omega,\text{offset}})}{mG} \qquad (1)$$

where $A_{2\omega,offset}$ is the lock-in offset, *m* the optical lever sensitivity and *G* the lock-in gain. Equation (1) comes from the relationships between the ac force and the oscillation amplitude in off-resonance, $F_{2\omega}=kA_{2\omega}$ and between the ac force and the capacitance gradient, dC/dz, $F_{2\omega}=1/4\ dC/dz\ v_{ac}^2$. SDM measurements were performed in controlled dry air environment conditions (RH < 1%) maintained by an N_2 flow.

Extraction of the equivalent homogeneous dielectric constant of the OMEs. The quantitative extraction of the equivalent homogeneous dielectric constant of the OMEs, ε_{eq}, was done following the standard methods of SDM (*21*), (*32*), (*33*). In a nutshell, we used finite element numerical calculations to simulate theoretical SDM capacitance gradient approach curves for a homogeneous dielectric model of the OMEs and fitted them to the experimental curves, with the equivalent homogeneous dielectric constant, ε_{eq}, being the single fitting parameter. The tip geometry (tip radius, half cone angle and capacitance gradient offset) was determined from *dC/dz* approach curves measured on a bare part of the metallic substrate as detailed elsewhere (*21*), (*32*), (*33*), (*35*). The following tip parameters were set to their nominal values: cone height $H = 12.5$ µm, local cantilever $L_c = 3$ µm and cantilever thickness $W_c = 3$ µm. The sample geometries for the OMEs and the bacterial cell body were directly reconstructed from the topographic images, as detailed elsewhere (*34*). Tip convolution effects were not accounted for explicitly, as they were assumed to have little effect in the extraction of the dielectric constant values since the probes tip radii were small (~20 nm) and the OMEs had a relatively large diameter ~ 50 nm –100 nm. The numerical calculations have been implemented in COMSOL Multiphysics 5.3a by using the AC/DC electrostatic module. The

quantitative analysis was carried by using a custom software routine written in Matlab (Math Works).

Analysis of the effects of the conductivity. To analyze the effects of an eventual conductivity of the OMEs in the magnitude of the capacitance gradient *dC/dz* and on the electric force dephasing we have considered the above-described model with a non-zero homogeneous conductivity, and solved it in the frequency domain by using the currents model implemented in the AC/DC electrostatic module of COMSOL Multiphysics 5.3a. The modulus and phase of the electric force have been determined by integration of the Maxwell stress tensor on the tip surface.

Conclusions

In this work, we have determined the dielectric properties of intact, non-chemically fixed, outer membrane extensions (OMEs) of *S. oneidensis MR-1* by means of Scanning Dielectric Microscopy (SDM) in force detection mode in a dry air environment. We have found that at a frequency of $\sim$ 2 kHz the OMEs show an insulating behavior with dielectric constant, $\varepsilon_{OME} = 3.7 \pm 0.7$. This value is compatible with the composition of OMEs being dominated by periplasmic proteins. Based on the sensitivity of the measuring instrument an upper conductivity limit was set to $\sigma_{OME} < 10^{-6}$ S/m, a value several orders of magnitude lower than the one measured on dry chemically fixed OMEs. We argued that the lack of conductivity in intact OMEs in dry air environment could be caused by the relatively large separation between cytochrome centers and to its reduced diffusivity due to the dry conditions. Present results do not preclude the occurrence of an eventual conductivity on hydrated intact OMEs, in which the mobility of the cytochromes is expected to be large enough for diffusion assisted hoping conduction.

Conflicts of interest

There are no conflicts to declare.

Acknowledgements

This work was partially supported by the Spanish Ministerio de Economía, Industria y Competitividad (MINECO) and EU FEDER through Grant No. PDI2019-110210GB-100 and and RTI2018-098573-B-100, the Generalitat de Catalunya through Grant No. 2017-SGR1079 and the CERCA Program. This work also received funding from the European Commission under Grant Agreement No. H2020-MSCA-721874 (SPM2.0). H.L. acknowledges support from MINECO through and FI grant (SEV-2014-0425-06). R.F. received funding from the Marie Sklodowska-Curie Action grant Nº 842402. We acknoweledge Prof. M. El-Naggar for his help in the growth of the OMEs.

References

1 D. R. Lovley, *Curr. Opin. Biotechnol.*, 2008, **19**, 564.
2 S. Kato, *Microbes Environ.,* 2015, **30**, 133.
3 G. F. White, M. J. Edwards, L. Gomez-Perez, D. J. Richardson, J. N. Butt, T. A. Clarke, *Adv. Microb. Physiol.*, 2016, **68**, 87.
4 D. R. Lovley, *Annu. Rev. Microbiol.*, 2012, **66**, 391.
5 G. Reguera, K. D. McCarthy, T. Mehta, J. S. Nicoll, M. T. Tuominen, D. R. Lovley, *Nature*, 2005, **435**, 1098.
6 Y. A. Y. Gorby, S. Yanina, J. S. McLean, K. M. Rosso, D. Moyles, A. Dohnalkova, T. J. Beveridge, I. S. Chang, B. H. Kim, K. S. Kim, D. E. Culley, S. B. Reed, M. F. Romine, D. A. Saffarini, E. A. Hill, L. Shi, D. A. Elias, D. W. Kennedy, G. Pinchuk, K. Watanabe, S. Ishii, B. Logan, K. H. Nealson, J. K. Fredrickson, *Proc. Natl. Acad. Sci. U.S.A.*, 2006, **103**, 11358.
7 M. Y. El-Naggar, G. Wanger, K. M. Leung, T. D. Yuzvinsky, G. Southam, J. Yang, W. M. Lau, K. H. Nealson, Y. A. Gorby, Proc. Natl. Acad. Sci. U.S.A., 2010, **107**, 18127.
8 N. S. Malvankar, M. Vargas, K. P. Nevin, A. E. Franks, C. Leang, B. C. Kim, K. Inoue, T. Mester, S. F. Covalla, J. P. Johnson, V. M. Rotello, M. T. Tuominen, D. R. Lovley, Nat. Nanotech., 2011, **6**, 573.
9 N. S. Malvankar, S. E. Yalcin, M. T. Tuominen, D. R. Lovley, Nat. Nanotech., 2014, **9**, 1012.
10 K. M. Leung, G. Wanger, M. Y. El-Naggar, Y. Gorby, G. Southam, W. M. Lau, J. Yang, Nano Letters, 2013, **13**, 2407.
11 S. M. Strycharz-Glaven, R. M. Snider, A. Guiseppi-Elie, L. M. T., Energy Environ. Sci., 2011, **4**, 4366.
12 S. Sure, M. J. Ackland, A. A. J. Torriero, A. Adholeya, M. Kochar, Microbiology, 2016, **162**, 2017.
13 D. R. Lovley, 2017,mBio, **8**, 1.
14 N. S. Malvankar, D. R. Lovley, Curr. Opin. Biotechnol., 2014, **27**, 88.
15 D. R. Lovley, J. Yao, Trends Biotechnol., 2021 (in press). https://doi.org/10.1016/j.tibtech.2020.12.005.
16 S. Pirbadian, S. E. Barchinger, K. M. Leung, H. S. Byun, Y. Jangir, R. A. Bouhenni, S. B. Reed, M. F. Romine, D. A. Saffarini, L. Shi, Y. A. Gorby, J. H. Golbeck, M. Y. El-Naggar, Proc. Natl. Acad. Sci. U.S.A., 2014, **111**, 12883.
17 P. Subramanian, S. Pirbadian, M. Y. El-Naggar, G. J. Jensen, Proc. Natl. Acad. Sci. U.S.A., 2018 **115**, E3246.
18 M. Toyofuku, N. Nomura, L. Eberl, Nat. Rev. Microbiol., 2019, **17**, 13.
19 S. Pirbadian, M. Y. El-Naggar, Phys. Chem. Chem. Phys., 2012, **14**, 13802.
20 K. M. Leung, G. Wanger, Q. Q. Guo, Y. Gorby, G. Southam, W. M. Lau, J. Yang, Soft Matter, 2011, **7**, 6617.
21 L. Fumagalli, D. Esteban-Ferrer, A. Cuervo, J. L. Carrascosa, G. Gomila, Nat. Mater., 2012, **11**, 808.
22 M. Bockrath, N. Markovic, A. Shepard, M. Tinkham, L. Gurevich, L. P. Kouwenhoven, M. W. Wu, L. L. Sohn, Nano Lett., 2002, **2**, 187.
23 W. Lu, D. Wang, L. W. Chen, Nano Lett., **7**, 2729-2733, 2007.
24 W. Lu, Y. Xiong, L. Chen, J. Phys. Chem. C, 2009, **113**, 10337.
25 Y. Yang, W. Guo, X. Wang, Z. Wang, J. Qi, Y. Zhang, Nano Lett., **12**, 2012, 1919.
26 H. Lozano, R. Millan-Solsona, R. Fabregas, G. Gomila, Sci. Rep., 2019, **9**, 74799.
27 O. Cherniavskaya, L. Chen, L. Weng, L. Yuditsky, L.-E. Brus, J. Phys. Chem. B, 2003, **107**, 1525.
28 A. Cuervo, P. D. Dans, J. L. Carrascosa, M. Orozco, G. Gomila, L. Fumagalli, Proc. Natl. Acad. Sci. U.S.A., 2014, **111**, E3624.
29 H. Lozano, R. Fabregas, N. Blanco-Cabra, R. Millan-Solsona, E. Torrents, L. Fumagalli, G. Gomila, Nanoscale, 2018, **10**, 19188.
30 H. T. S. Boschker, P. L. M. Cook, L. Polerecky, R. T. Eachambadi, H. Lozano, S. Hidalgo-Martinez, D. Khalenkow, V. Spampinato, N. Claes, P. Kundu, D. Wang, S. Bals, K. K. Sand, F. Cavezza, T. Hauffman, J. T. Bjerg, A. Skirtach, K. Kochan, M. McKee, B. Wood, D. Bedolla, A. Gianoncelli, N. M. J. Geerlings, N. Van Gerven, H. Remaut, J. S. Geelhoed, R. Millan-Solsona, L.

Fumagalli, L. P. Nielsen, A. Franquet, J. V. Manca, G. Gomila, F. J. R. Meysman, Nat. Commun., 2021, **12**, 3996.
31 D. Esteban-Ferrer, M. A. Edwards, L. Fumagalli, A. Juarez, G. Gomila, ACS Nano, 2014, **8**, 9843.
32 L. Fumagalli, G. Ferrari, M. Sampietro, G. Gomila, Appl. Phys. Lett., **91**, 2007, 243110.
33 L. Fumagalli, G. Gramse, D. Esteban-Ferrer, M. A. Edwards, G. Gomila, Appl. Phys. Lett., **96**, 2010, 183107.
34 M. Checa, R. Millán-Solsona, N. Blanco-Cabra, E. Torrents, R. Fábregas, G. Gomila, Nanoscale, **11**, 2019, 20809.
35 G. Gramse, G. Gomila, L. Fumagalli, Nanotechnology, 2012, **23**.
36 M. Van Der Hofstadt, R. Fabregas, M. Biagi, L. Fumagalli, G. Gomila, Nanotechnology, 2016, **27**, 405706.
37 A. Dols-Perez, G. Gramse, A. Calo, G. Gomila, L. Fumagalli, Nanoscale, 2015, **7**, 18327.
38 G. Gramse, M. A. Edwards, L. Fumagalli, G. Gomila, Appl. Phys. Lett., 2012, **101**, 213108.
39 G. Gramse, A. Dols-Perez, M. A. Edwards, L. Fumagalli, G. Gomila, Biophys. J., 2013, **104**, 1257.
40 M. Di Muzio, R. Millan-Solsona, J. H. Borrell, L. Fumagalli, G. Gomila, Langmuir, **36**, 2020, 12963.
41 R. Millan-Solsona, M. Checa, L. Fumagalli, G. Gomila, Nanoscale, 2020, **12**, 20658.
42 M. Di Muzio, R. Millan-Solsona, J. H. Borrell, L. Fumagalli, G. Gomila, J. Nanobiotech., 2021, **19**, 1.
43 A. Kyndiah, M. Checa, F. Leonardi, R. Millan-Solsona, M. Di Muzio, S. Tanwar, L. Fumagalli, M. Mas-Torrent, G. Gomila, Adv. Func. Mat., 2021, **31**, 2008032.

Supplementary information of

Electrical Properties of Outer Membrane Extensions from *Shewanella Oneidensis* MR-1

H. Lozano[1], R. Millan-Solsona[1,2], N. Blanco-Cabra[3], R. Fabregas[4], E. Torrents[3,5], and G. Gomila[1,2]

[1]Nanoscale Bioelectrical Characterization, Institute for Bioengineering of Catalonia (IBEC), The Barcelona Institute of Science and Technology (BIST), Baldiri i Reixac 11-15, 08028, Barcelona, Spain

[2]Departament d'Enginyeria Electrònica i Biomèdica, Universitat de Barcelona, Martí i Franqués 1, 08028, Barcelona, Spain

[3]Bacterial Infections: Antimicrobial Therapies, Institute for Bioengineering of Catalonia (IBEC), The Barcelona Institute of Science and Technology (BIST), Baldiri i Reixac 11-15, 08028, Barcelona, Spain

[4]School of Physics and Astronomy, University of Manchester, Manchester M13 9PL, UK

[5]Departament de Genètica, Microbiologia i Estadística, Universitat de Barcelona, Av. Diagonal 643, 08028, Barcelona, Spain

S1. Additional data to Figure 1a.

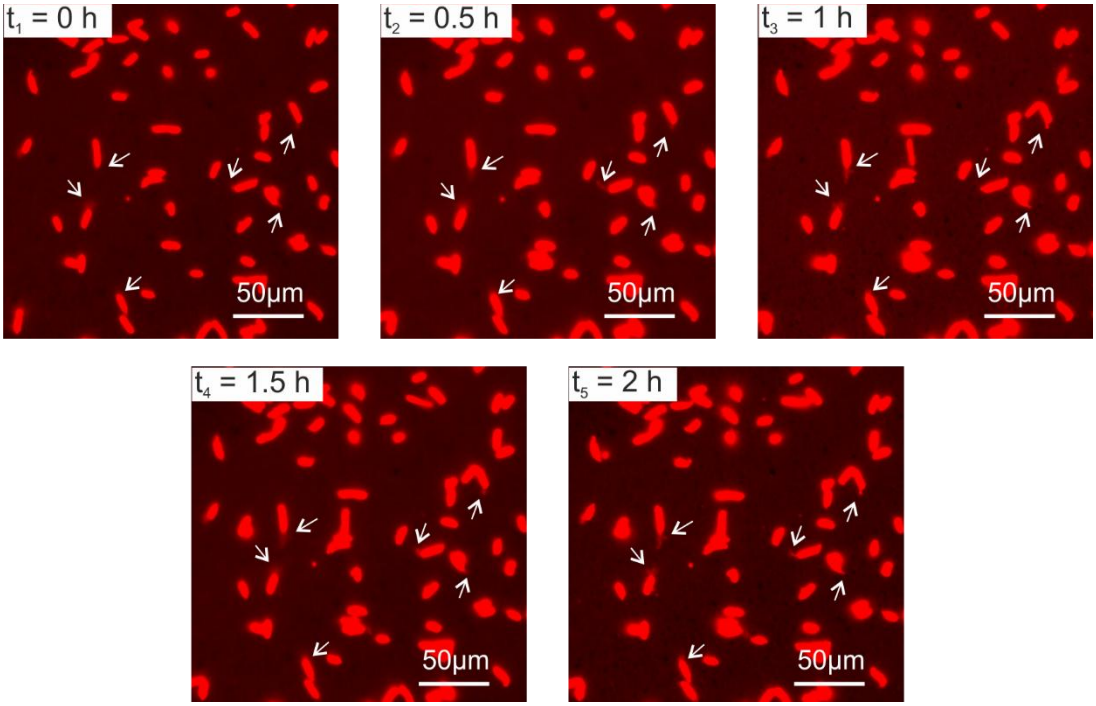

Figure S1*: Time sequence of fluorescence light microscope images of S. oneidensis bacterial cells labelled with the membrane dye* FM™-464FX. *White arrows point towards some of the OMEs.*

S2. Effect of hydration on the OMEs physical dimensions

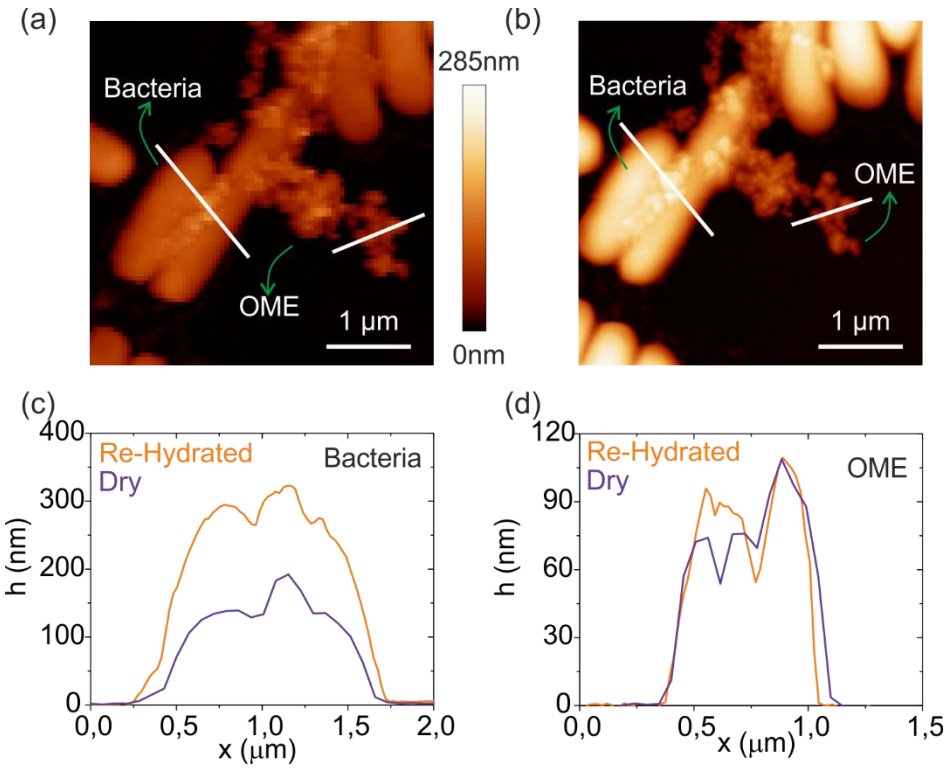

***Figure S2**: (a) and (b) AFM topography images of S. oneidensis bacterial cells with OMEs adsorbed on a glass substrate in dry air and fully re-hydrated conditions, respectively. (c) and (d) Topographic cross-section profiles of the bacterial cell and of the OMEs, respectively, in air and re-hydrated conditions along the lines in (a) and (b). While the bacterial cell nearly doubles its size upon-rehydration, OMEs remain almost unaffected.*

S3. Additional data to Figure 2c

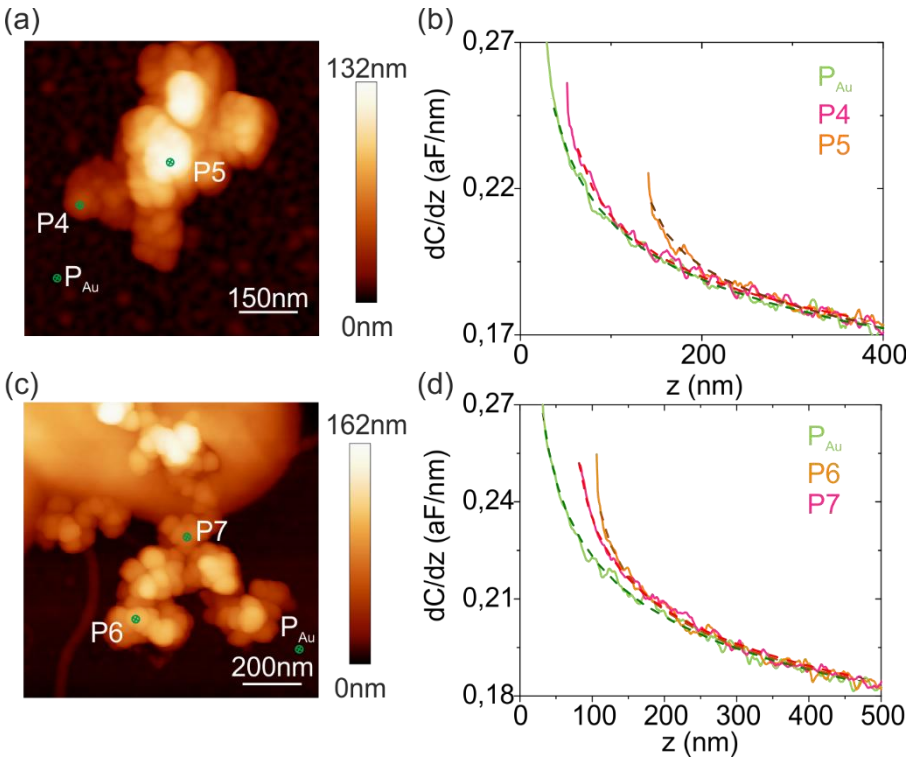

***Figure S3**: (a) and (c) AFM topographic images of two Shewanella oneidensis OMEs, and (b) and (d) corresponding capacitance gradient curves measured at selected positions. The dashed lines represent the theoretically fitted curves, from where the tip geometry and the equivalent homogeneous dielectric constants have been extracted. Parameters for (a) and (b): tip PtSi-CONT, k = 0.4 N/m, V_{ac} = 5 V, f_{el} = 2kHz, R = 31 ± 2 nm, ϑ = 22 ± 3°, C'_{offset} = 88 ± 1 aF/nm, ε_{OME} = 3.6 ± 0.1. Parameters for (c) and (d): tip PtSi-CONT, k = 0.3 N/m, V_{ac} = 5 V, f_{el} = 2kHz, R = 25 ± 2 nm, ϑ = 22 ± 3°, C'_{offset} = 103 ± 1 aF/nm, ε_{OME} = 4.3 ± 1.0.*

S4. Additional data to Figure 3.

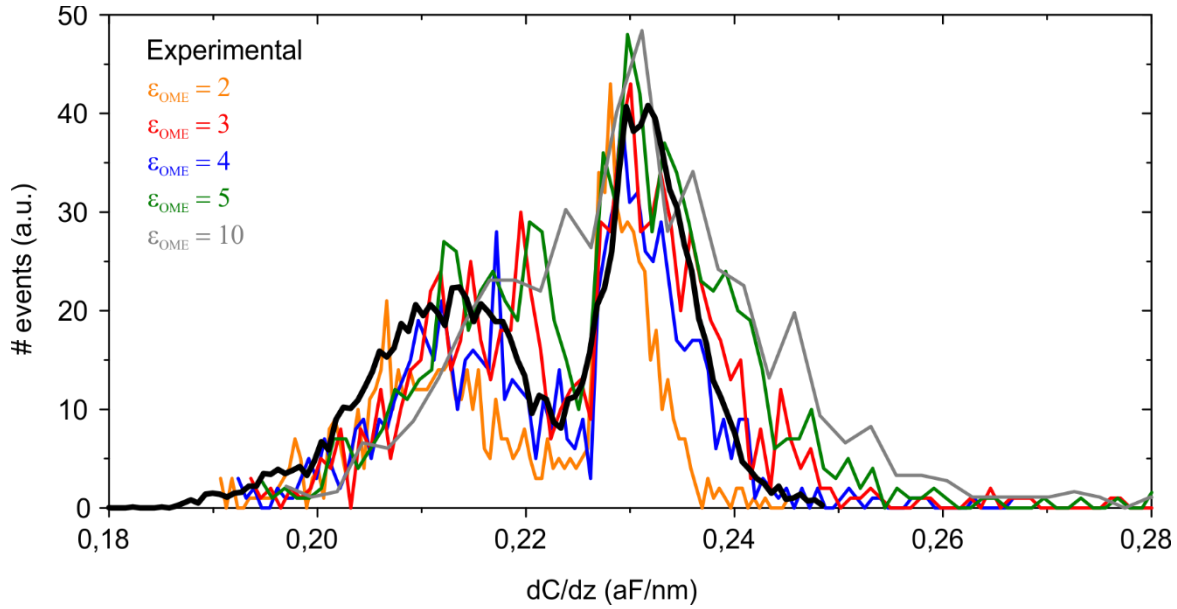

***Figure S4**: Histogram analysis of the experimental lift-mode dC/dz SDM image shown in Fig. 3b of the main text (black line), and the theoretically calculated ones shown in Figs. 3h-3l corresponding to equivalent homogeneous dielectric constants ε_{OME} = 2, 3, 4, 5, 10 (remaining lines). The best agreement is found for ε_{OME} = 3 – 4 (red and blue lines).*

S5. Effect of the shell conductivity on the dC/dz values for a core-shell model of the OMEs.

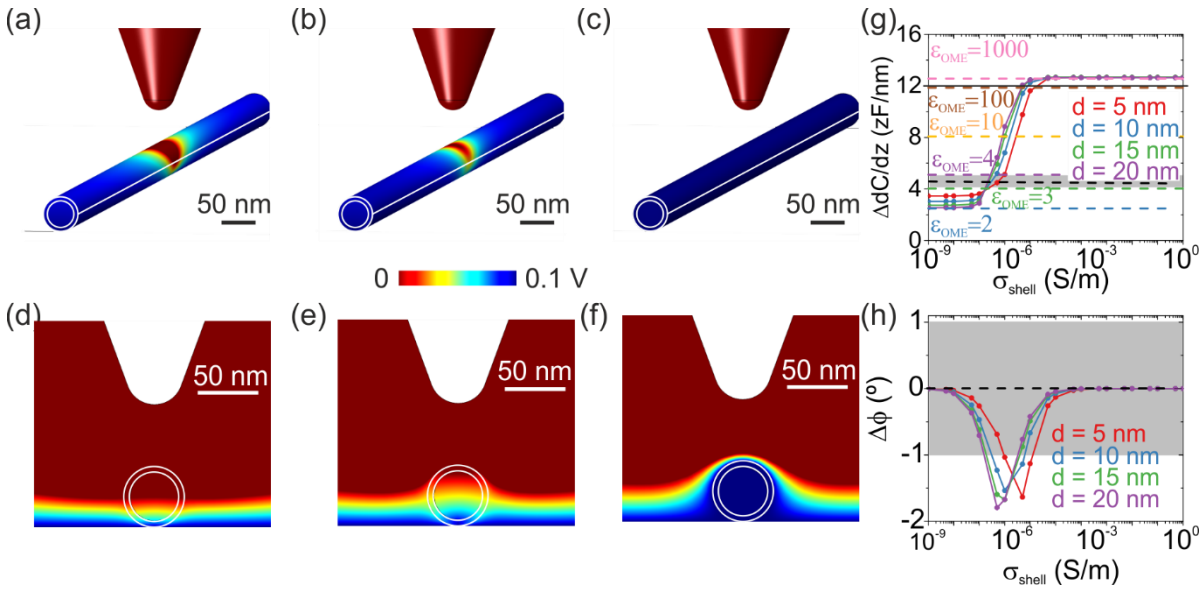

Figure S5*: Calculated electric potential distributions on the surface (a)-(c) and cross-section (d)-(f) of a cylindrical conductive core-shell model of an OME for three characteristic homogeneous conductivities of the shell* $\sigma_{shell} = 10^{-9}$ *S/m (insulator),* $\sigma_{shell} = 2.5 \cdot 10^{-6}$ *S/m (insulator with losses) and* σ_{shell}*=1 S/m (conductor). (g) Capacitance gradient contrast and (h) dephasing as a function of the conductivity of the shell,* σ_{shell}*, for four different values of the thickness of the shell (d = 5 nm, 10 nm, 15 nm and 20 nm). The black dashed lines correspond to the value of a homogeneous dielectric model with the experimentally found equivalent homogeneous dielectric constant (*$\varepsilon_{eq} = 3.7$*). The remaining dashed lines correspond to the indicated values in the figure. The grey areas correspond to the uncertainty in the measurements due to the noise of the measuring set-up. Parameters used in the calculations: width and height of the OME* $h_{OME} = w_{OME} = 50$ *nm, length of the OME* $L_{OME} = 4$ *µm, tip-sample distance = 50 nm,* ε_{core}*=3,* ε_{shell}*=2,* σ_{core}*=0 S/m, R = 23 nm,* $\vartheta = 20°$*, H = 12.5 µm,* $L_c = 3$ *µm and* $W_c = 3$ *µm*.

S6. OMEs growth reactor

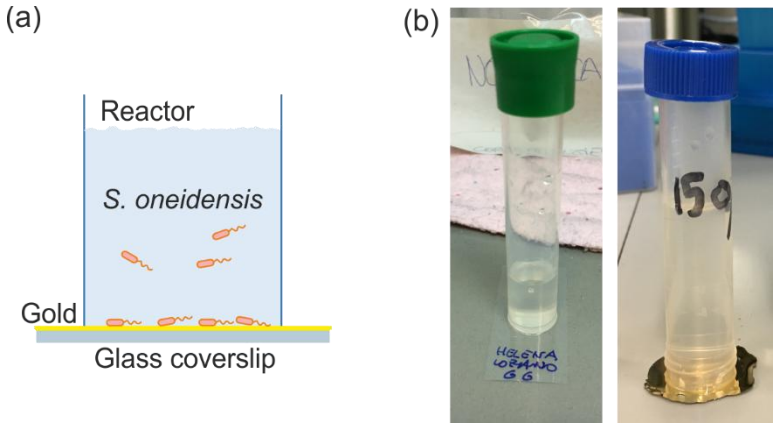

Figure S6*: (a) Schematic representation of the reactor used to growth the OMEs. (b) Pictures of the reactor set-up used with a glass coverslip and a gold-coated glass coverslip.*